Structural Dynamics Analysis of ATPS Parachute using Nonlinear Finite Element method

Ying Tong, Fan Liu*, Lu Zhang, Yongfei Mou

China Aerodynamic Research and Development Center, Mianyang, Sichuan, 621000, China

* Corresponding Author Email: liuf07@cardc.cn

Abstract. A computational structural dynamics method based on the nonlinear finite element (NFE) model is developed for simulating the dynamic response of parachutes. Numerical simulation results for benchmark cases and ASTM parachute inflation demonstrate the advantages of the proposed method in terms of comparable accuracy, perfect convergence, superior algorithmic stability, and stronger ability to handle highly nonlinear equations. Compared with the existing numerical methods used in parachute simulation, the proposed method can capture the more real mechanical behaviour of parachute by introducing the nonlinear factors in the physical model involved into the governing equation entirely, then using the nonlinear theory to build the calculation model, last solving the equivalent linear equations.

Keywords: Nonlinear Finite Element Method, ATPS Parachute, Structural Dynamics.

1. Introduction

With the increasing application of parachute pneumatic retarders in the engineering, the importance of fluid-structure interaction (FSI) dynamic effect of this kind of special entity becomes more and more prominent. Because flexible fabric materials are extremely sensitive to air loads, the mechanical model of a parachute in service involves multiple nonlinear sources, such as geometric nonlinearity and nonconservative loads. These make numerical simulations of parachutes a challenging research topic for the CSD community.

The tension structures (membrane and cable) [1] composing parachute is a special bearing component in aeronautics, astronautics and other fields. It transfers the load imposed on the bearing surface to the transverse foundation surface or other supporting structure by direct tensile stress, without bending or compression in the bearing direction. From the perspective of solid mechanics, the membrane-cable entities essentially have a larger slenderness ratio than the thin flexible bodies of plates or shells, and their bending stiffness is close to zero. These particular geometrical sizes and mechanical properties give it a stronger nonlinear character compared to the plate/shell entities. In order to capture the nonlinear behavior of parachute under air load as much as possible and improve the structural dynamic analysis ability of simulation technology for such special entities, it is necessary to develop a numerical simulation method which is more stable than the plate/shell model and has a stronger ability to deal with nonlinear equations.

In this paper, we develop a numerical simulation method for parachute inflation. The physical model of continuous membrane-cable entities is based on the finite deformation theory of 3D entities [2]. The motion of the particle is described by the total Lagrangian method and random coordinates. We derive the governing equations of motion for continuous membrane-cable systems based on the D'Alembert-Lagrange principle [3]. The range of applications of the governing equations is not subject to any assumptions other than those inherent to the kinematic assumptions of the structural model [4]. By introducing a generalized-α implicit time integration algorithm [5], the original numerical scheme is improved with a numerical damping addition strategy, which improves the performance in both high and low frequency bands. Numerical simulation results show that the proposed approach significantly improves the predictive ability of the simulation technique for the structural dynamical response of parachutes.

2. Method

According to the finite deformation theory in continuum mechanics [2], we established a structural dynamics model described by tensor system. As shown in Figure 1, the particle motion is described by using convected curved coordinates ξ^i.

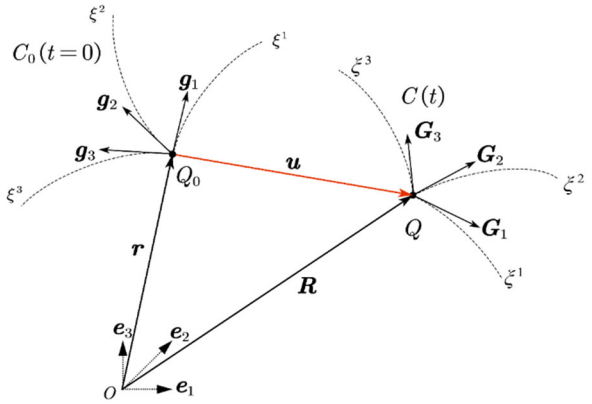

Figure 1. The convected coordinate description of particle motion.

The second type of Kirchhoff stress tensor and Green's strain tensor are used to measure the stress and strain of the parachute. After time *t*, the differential length ds_0 at initial time changes to ds. $\boldsymbol{g}_i$ and $\boldsymbol{G}_i$ are the covariant basis vectors of the material points in reference configuration C_0 and current configuration C. The Green's strain tensor $\boldsymbol{E}$ is defined by the differential length change:

$$\begin{aligned} ds^2 - ds_0{}^2 &= 2E_{ij}d\xi^i d\xi^j \\ E_{ij} &= \frac{1}{2}(G_{ij} - g_{ij}) \end{aligned} \tag{1}$$

Here, g_{ij} and G_{ij} are covariant components of the metric tensor in C_0 and C, respectively. E_{ij} is the covariant component of Green's strain tensor $\boldsymbol{E}$.

The contravariant component of the second type of Kirchhoff stress tensor Σ is as follows:

$$\Sigma^{ij} = \left\{ \frac{E\nu}{(1+\nu)(1-2\nu)} g^{ij}g^{kl} + \frac{E}{2(1+\nu)}\left(g^{ik}g^{jl} + g^{il}g^{jk}\right) \right\} E_{lk}, \quad \forall i,j,k,l = 1,2,3 \tag{2}$$

where E is the elastic modulus, g^{ij} is the contravariant component of the medium metric tensor.

Using the total Lagrangian approach, at time t=0, the initial configuration with no strain and known configuration is taken as the reference configuration C_0. The movement of the parachute and the virtual work of the system forces (such as, inertial force, internal force, and external force) are relative to the definition. Based on the D'Alembert principle [3], the motion equations of continuous system can be established:

$$\int_{V_0} \Pi^{ij}\delta E_{ij}dV_0 + \int_{V_0} \rho_0 \ddot{u}_i \delta u_i dV_0 - \int_{V_0} f_{0i}\delta u_i dV_0 - \int_{S_0} t_{0i}\delta u_i dS_0 = 0 \tag{3}$$

where, ρ_0 refers to the material density defined by unit volume entity in C0; $\ddot{u}_i$ is the acceleration of the particle at time t; f_{0i} represents the projection of the volume force in C onto C0, $f_{0i}dV_0 = f_i dV$; t_{0i} comes from the projection of the surface force in C, $t_{0i}dS_0 = t_i dS$. Different from the traditional linear elastic hypothesis, Eq.(3) is valid for any size of displacement or strain, and is not limited to linear stress-strain relationship.

By matching the membrane-cable elements in the finite element model to the global equations [6], the system motion differential equations in matrix form can be obtained:

$$\boldsymbol{M}\ddot{\boldsymbol{U}}+\boldsymbol{C}\dot{\boldsymbol{U}}+\boldsymbol{R}-\boldsymbol{F}=0\,. \tag{4}$$

Here, $\boldsymbol{M}$ is the mass matrix, $\ddot{\boldsymbol{U}}$ and $\dot{\boldsymbol{U}}$ are the acceleration and velocity vector, $\boldsymbol{F}$ is the external force vector, and $\boldsymbol{R}$ is the internal force vector.

The generalized-α implicit time advance scheme [5] is used to solve Eq.(4); the generalized-α scheme integrates the characteristics of Newmark method, HHT-α method and WBZ-α method. By adjusting the numerical parameters, the numerical damping with fast attenuation (filtering false high-order modes) can be guaranteed in the high frequency band, and the numerical damping with slight control can be added in the low frequency band (ensuring the accuracy of the numerical solution).

The generalized-α scheme uses the following relations to describe the velocity and displacement vector at $t+\Delta t$:

$$\begin{aligned}\dot{\boldsymbol{U}}_{t+\Delta t}&=\dot{\boldsymbol{U}}_t+(1-\gamma)\ddot{\boldsymbol{U}}_t\Delta t+\gamma\ddot{\boldsymbol{U}}_{t+\Delta t}\Delta t\\ \boldsymbol{U}_{t+\Delta t}&=\boldsymbol{U}_t+\dot{\boldsymbol{U}}_t\Delta t+\left(\frac{1}{2}-\beta\right)\ddot{\boldsymbol{U}}_t\Delta t^2+\beta\ddot{\boldsymbol{U}}_{t+\Delta t}\Delta t^2\end{aligned} \tag{5}$$

The generalized-α scheme calculate $\boldsymbol{U}_{t+\Delta t}$ using the following govern equations:

$$\begin{aligned}(1-\alpha_m)[\boldsymbol{M}]\{\ddot{\boldsymbol{U}}_{t+\Delta t}\}+\alpha_m[\boldsymbol{M}]\{\ddot{\boldsymbol{U}}_t\}+(1-\alpha_f)[\boldsymbol{C}]\{\dot{\boldsymbol{U}}_{t+\Delta t}\}+\alpha_f[\boldsymbol{C}]\{\dot{\boldsymbol{U}}_t\}\\ +(1-\alpha_f)\{\boldsymbol{R}_{t+\Delta t}-\boldsymbol{F}_{t+\Delta t}\}+\alpha_f\{\boldsymbol{R}_t-\boldsymbol{F}_t\}=0\end{aligned} \tag{6}$$

According to the increment-iteration method [7], combined with Eq.(5) and Eq.(6), the system equivalent linear equations of generalized-α scheme are constructed as follows:

$$\begin{aligned}&\left(\frac{1}{\beta\Delta t^2}(1-\alpha_m)[\boldsymbol{M}]+\frac{\gamma}{\beta\Delta t}(1-\alpha_f)[\boldsymbol{C}]+(1-\alpha_f)[{}^{n}_{m+1}\boldsymbol{K}_{t+\Delta t}]\right)\{{}^{n}_{m+1}\Delta\boldsymbol{U}_{t+\Delta t}\}\\ &=(1-\alpha_f)\left\{{}^{n}_{m+1}\boldsymbol{F}_{t+\Delta t}-{}^{n}_{m+1}\boldsymbol{R}_{t+\Delta t}\right\}+\alpha_f\left\{\boldsymbol{F}_t-\boldsymbol{R}_t\right\}\\ &\quad-[\boldsymbol{M}]\left((1-\alpha_m)\left(\frac{1}{\beta\Delta t^2}\left\{{}^{n}_{m+1}\boldsymbol{U}_{t+\Delta t}-\boldsymbol{U}_t\right\}-\frac{1}{\beta\Delta t}\left\{\dot{\boldsymbol{U}}_t\right\}-\left(\frac{1}{2\beta}-1\right)\left\{\ddot{\boldsymbol{U}}_t\right\}\right)+\alpha_m\left\{\ddot{\boldsymbol{U}}_t\right\}\right)\\ &\quad-[\boldsymbol{C}]\left((1-\alpha_f)\left(\frac{\gamma}{\beta\Delta t}\left\{{}^{n}_{m+1}\boldsymbol{U}_{t+\Delta t}-\boldsymbol{U}_t\right\}+\left(1-\frac{\gamma}{\beta}\right)\left\{\dot{\boldsymbol{U}}_t\right\}+\left(1-\frac{\gamma}{2\beta}\right)\Delta t\left\{\ddot{\boldsymbol{U}}_t\right\}\right)+\alpha_f\left\{\dot{\boldsymbol{U}}_t\right\}\right)\end{aligned} \tag{7}$$

Here, the initial calculated value at time $t+\Delta t$ is set by the convergence solution at time t: ${}^{0}_{0}\boldsymbol{U}_{t+\Delta t}=\boldsymbol{U}_t$. The initial iteration value after each load advance update is set by the iterative convergence solution under the previous load condition: ${}^{0}_{m+1}\boldsymbol{U}_{t+\Delta t}={}^{n}_{m}\boldsymbol{U}_{t+\Delta t}$.

3. Benchmark Cases Numerical Verification

3.1 Gravity driven suspension dynamic response

According to the conditions of experiments and simulations in literatures [8-10], dynamic response simulation of suspension cable was performed. The suspension cable (Length L=1 m, cross section area A= 1.0×10^{-4} m^2, elasticity modulus E=5.0×10^{6} pa, density ρ=1.0×10^{3} kg/m^3) fixed at one end, side of freedom. Fig. 2 shows the resulting statically balanced configuration with dead weight as input condition and the right end of the cable placed at a position with a horizontal span of 0.881L.

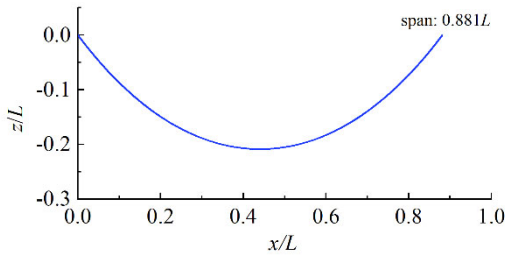

Figure 2. The statically balanced configuration of the suspension cable considering dead weight.

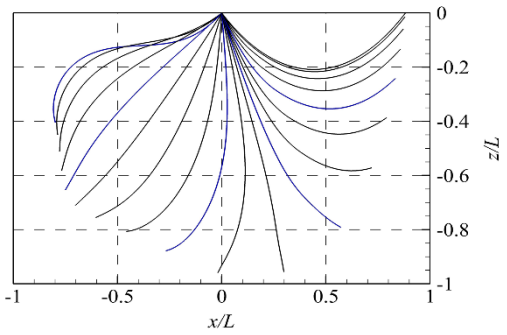

Figure 3. Dynamic response of suspension cable released from the horizontal span of 0.881L.

The NFE simulation was performed in the initial state of the statically balanced suspension cable as shown in Figure 2. Figure 3 shows the time history of the real configuration of the suspension cable after 1s release. Here, the blue cable configuration corresponds to the experimental record results of the literature [10]. It can be found that these simulation results are in good agreement with the experimental record.

3.2 Square membrane under static pressure

In this section, the simulation corresponding to dynamic experiment of a square membrane under static pressure reported by Shi et al. [11] was performed. Figure 4 shows the initial geometry, static pressure loading pattern, boundary conditions, and sampling point locations of the square membrane. According to the experimental parameters in reference [11], the size parameters of square membrane are: length L=0.406 m, thickness t=1.6×10^{-4} m. The square membrane is made of DuPont^{TM} Tyvek material with material properties of E=8.75×10^{8} Pa, ν=0.24, ρ=1.0×10^{3} kg/m^{3}.

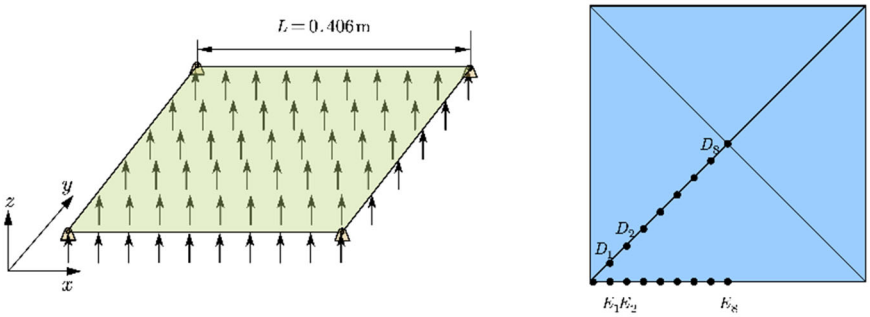

Figure 4. NFE simulation parameter setting of square membrane dynamic response.

To illustrate the grid convergence of the current results, the sensitivity analysis of the simulation results was performed using the grid convergence index (GCI) method [12]. Table 1 lists the sensitivity analysis results for the max deflection H of the membrane based on three sets of grid resolution and four static pressure situations (P_{int}=25, 50, 100 and 150 Pa). According to the data, the max deflection results from 20×20 quad-elements complete convergence those results from the 40×40 quad-elements. So, the subsequent simulations are performed using 20×20 quad-elements. In addition, the convergence rate calculated from the slope between the L_2 norm of the max deflection H in logarithmic coordinates and the grid resolution (h=L/5, L/10, L/20, and L/40) is approximately 2.0. It shows that the numerical solution obtained from the generalized-α implicit integration scheme with second-order accuracy.

Table 1. Grid sensitivity analysis of square membrane under static pressure.

P_{int}/Pa	Numerical results of Max deflection *H/mm*			$\frac{GCI_{23}}{r^p GCI_{12}}$	Convergence results of Max deflection *H/mm*
	h_1	h_2	h_3		
	L/40	*L*/20	*L*/10		
25	11.936	11.936	11.392	1.000	11.936
50	15.209	15.209	14.503	1.000	15.209
100	19.232	19.232	18.356	1.000	19.232
150	22.024	22.024	21.036	1.000	22.025

Based on the three groups of implicit integration scheme (Newmark, HHT-α, generalized-α), Figure 5 shows the phase diagram of maximum deflection *H* and static pressure P_{int} and compares with the literature's results [13-16]. It can be seen that when static pressure is minor (P_{int}=25 Pa), the linear theoretical results are in good agreement with the experimental results. This is because the membrane response is mainly linear under a minor external loading. In this case, the damping introduced by the numerical model taking into account the geometric nonlinearity makes the results deviate from the true solution. When the static pressure is increased to 50 Pa or more, the large deformation of the system leads to nonlinear effects dominating the motion and deformation. In this case, the linear theoretical model results deviate significantly from the experimental results and the linearity assumption is invalid. On the other hand, NFE models that take into account geometric nonlinearities can provide reliable response predictions for the membrane. For $P_{int}\in$[50,150], the simulation results based on three groups of implicit integration scheme are coincide, and the maximum deflection predicted in the tolerance range. In addition, the deflection obtained by using the quadratic element in the NFE model is comparable to that obtained by using the S3 triangle element in the FEM/Membrane model based on ABAQUS commercial software, but the total degree of freedom simulated in this paper is only 1/3 of the total degree of freedom of the reference model. Clearly, the current model does a better job of calculating the cost.

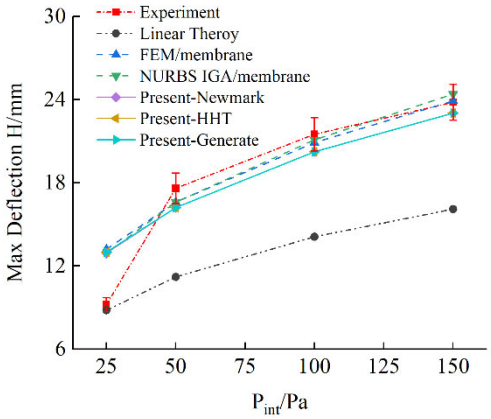

Figure 5. Phase diagram of the max deflection H and the static pressure P_{int}.

Figure 6 shows the deflection of the material points D_1-D_8 on the diagonal and E_1-E_8 on the edge obtained at constant pressure P_{int}=100 Pa based on three sets of implicit integration schemes and compares the results with those in the existing literature. It can be seen that the diagonal deflection prediction obtained is in good agreement with the numerical results in the literature [16]. Figure 7 shows the contours of the square membrane in a dynamically balanced configuration at static pressure P_{int}=100 Pa. The dynamically balanced configurations obtained with the three integration schemes for the membrane response are not significantly different. Here, we only show the simulation results based on the generalized-α integration.

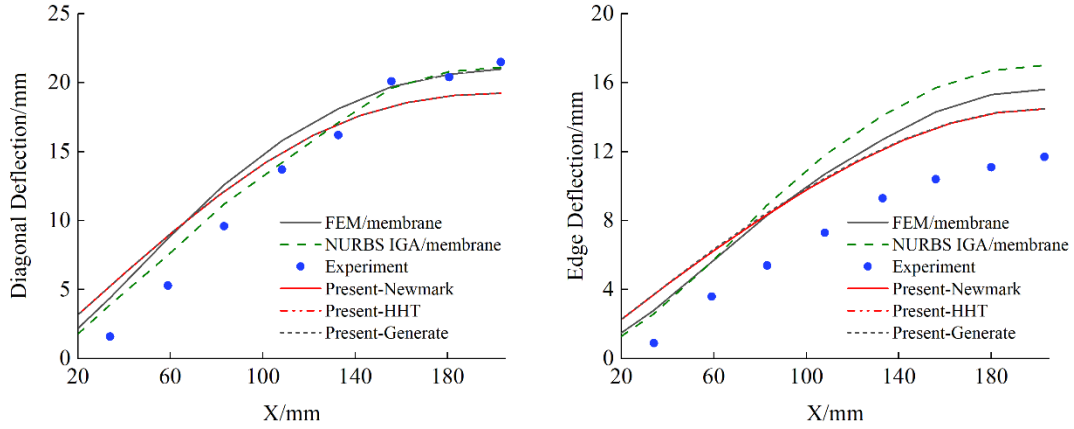

(a) Deflection of D_1-D_8 on the diagonal (b) Deflection of E_1-E_8 on the edge

Figure 6. The deflection of the sampling point on the square membrane at P_{int}=100 Pa.

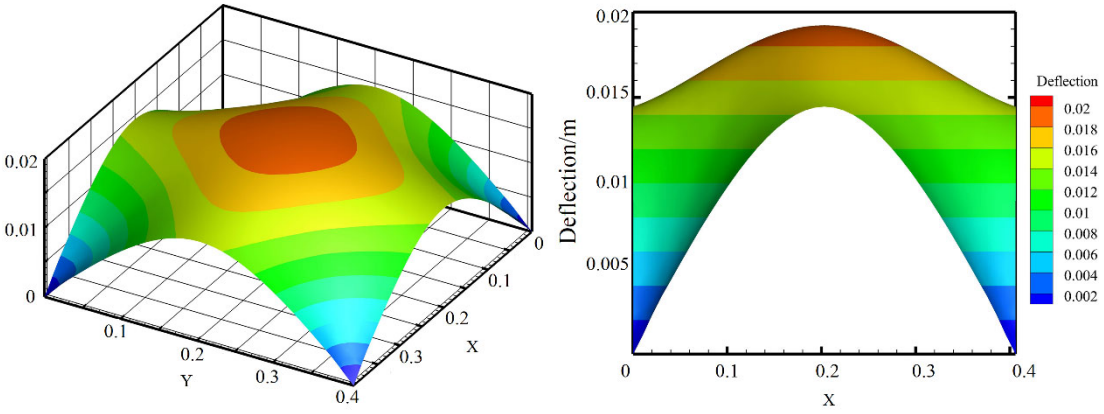

(a) 3D space diagram (b) Front view diagram

Figure 7. Dynamic balanced configuration of square membrane at P_{int}=100 Pa.

4. ATPS concept parachute inflation simulation

To test the capabilities of the solver developed to handle complex engineering problems, the inflation process of the ATPS concept parachute [17] is simulated. The material properties of the canopy are as follows: E=9.5695 MPa, ν=0.3, t=3.048×10^{-5} m, ρ=1223.5093 kg/m^3. The material properties of the cables are as: E=534.45 MPa, ν=0.3, ρ=1223.5093 kg/m^3, A=3.119×10^{-6} m^2. For the convenience of comparison, we set the numerical simulation aerated dynamic pressure loading P=1.3P_0 by referring to the experimental parameters given in literature [17], where the stagnation point pressure P_0 is based on the calculation of the experimental steady drop velocity of 4.8768m/s.

Figure 8 shows the instantaneous geometry of the ATPS parachute inflation process within 0.2 s. The ATPS parachute expands from its initial configuration and rapidly evolves to an expanded configuration protruding from the top of the canopy under the coupling effects of dead weight, rope bottom loading, and dynamic pressure loading. The canopy then begins to contract, the canopy gradually sinks to a flat state, and the top undergoes over-expansion again. The above dynamic process is repeated, presenting the classic “breathing phenomenon” in wind tunnel experiment records.

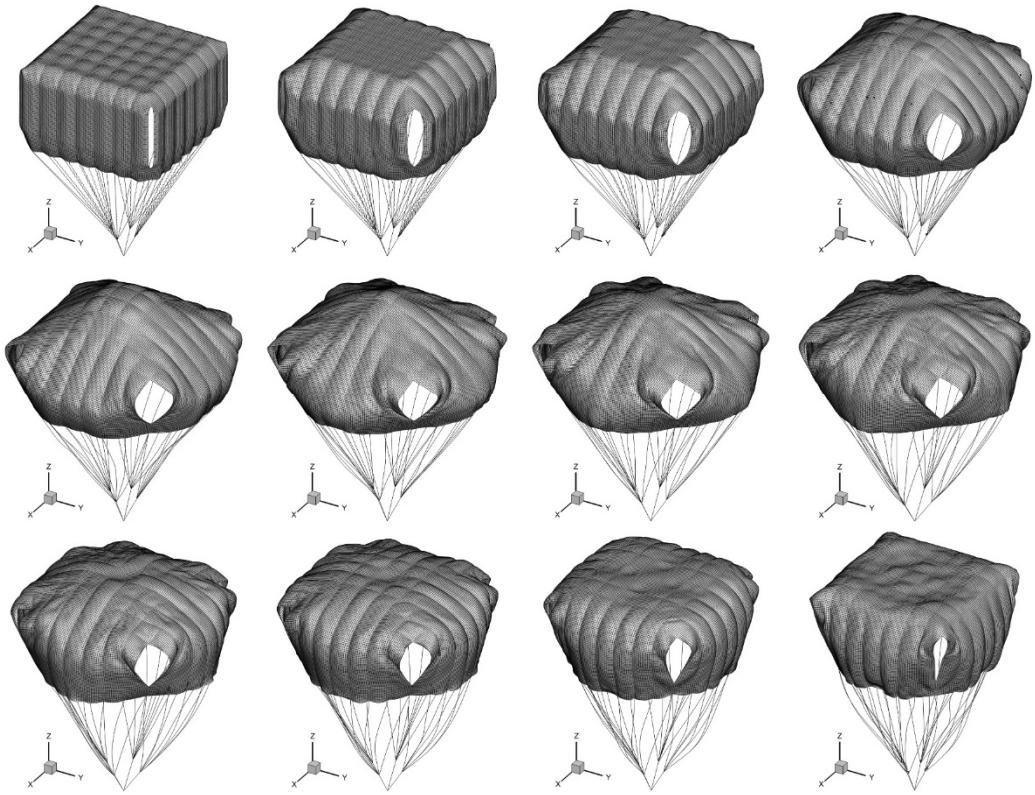

Figure 8. Dynamic inflation process of ATPS parachute.

Figure 9 shows the dynamic balance configuration of ATPS parachute, and the simulation results of Sathe et al. [17] are also shown. It can be found that our simulation results are highly consistent with the reference, which verifies the reliability of the results and the robustness and practicability of the solver developed in the modeling and simulation of complex structural dynamics problems.

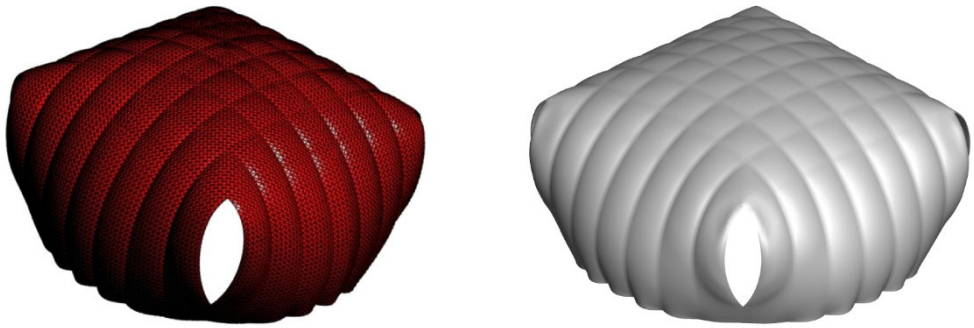

(a) Reference literature result (b) Simulation result

Figure 9. Dynamic balance configuration of ATPS parachute.

5. Conclusion

In this paper, the proposed and developed NFE-CSD method can be applied to the nonlinear response analysis of tensioned membrane-cable entities under nonconservative loads. This method can obtain the numerical results which are in good agreement with the experimental results. Simulation results on benchmark cases show that the proposed approach has the advantages of comparable computational accuracy, good convergence, high algorithmic stability, and stronger numerical tractability for nonlinear algebraic equations compared to traditional numerical methods. Numerical simulations of the parachute inflation process demonstrate the ability of the developed solver to capture the more realistic dynamical behavior of the membrane-cable parachute system,

validating the robustness and practicality of the numerical treatment scheme in modeling and simulating complex structural dynamics problems.

Acknowledgments

This work was financially supported by the Nature Foundation Youth Fund project "Research on Parachute Fluid-Structure Coupling Simulation Method based on Absolute Node-coordinate Method and Lattice Boltzmann Flux Solver" (Foundation No. 12102446).

References

[1] Lewis, W.J., Tension structures: form and behaviour[M]. Thomas Telford, 2003.

[2] Lo, A. Nonlinear dynamic analysis of cable and membrane structures[D]. Oregon State University, 1982.

[3] Xiong Zhang, Tianshu Wang, Computational Dynamics[M]. Beijing: Tsinghua University Press, 2007

[4] Le Van, A., Nonlinear Theory of Elastic Plates[M]. Elsevier, 2017

[5] Chung, J. and G.M. Hulbert. A time integration algorithm for structural dynamics with improved numerical dissipation: the generalized-α method[J], Journal of Applied Mechanics, 1993. 60(2): p. 371.

[6] Belegundu, Ashok D . Introduction to finite elements in engineering[M]. China Machine Press, 2013.

[7] Youquan Ying. Nonlinear finite element basis [M]. Beijing: Peking University Press, 2007

[8] Coyette, J. and P. Guisset. Cable network analysis by a nonlinear programming technique[J], Engineering Structures, 1988. 10(1): p. 41-46.

[9] Fried, I. Large deformation static and dynamic finite element analysis of extensible cables[J], Computers & Structures, 1982. 15(3): p. 315-319.

[10] Lazzari, M., A.V. Saetta, and R.V. Vitaliani. Non-linear dynamic analysis of cable-suspended structures subjected to wind actions[J], Computers & Structures, 2001. 79(9): p. 953-969.

[11] Shi, X. and E. Burnett. Mechanics and test study of flexible membranes ballooning in three dimensions[J], Building and Environment, 2008. 43(11): p. 1871-1881.

[12] Kwaśniewski, L. Application of grid convergence index in FE computation[J], Bulletin of the Polish Academy of Sciences: Technical Sciences, 2013(1).

[13] Shi, X. and E. Burnett. Mechanics and test study of flexible membranes ballooning in three dimensions[J], Building and Environment, 2008. 43(11): p. 1871-1881.

[14] Shi, X., J. Liang, and E. Burnett. Mechanics and test study of two-dimensional flexible membranes[J], Journal of Architectural Engineering, 2006. 12(2): p. 93-99.

[15] Wang, S., et al. Nonlinear 3D numerical computations for the square membrane versus experimental data[J], Engineering Structures, 2011. 33(5): p. 1828-1837.

[16] Chen, L., et al. Explicit finite deformation analysis of isogeometric membranes[J], Computer Methods in Applied Mechanics and Engineering, 2014. 277: p. 104-130.

[17] Sathe, S., et al. Fluid–structure interaction modeling of complex parachute designs with the space–time finite element techniques[J], Computers & Fluids, 2007. 36(1): p. 127-135.